Supporting information for:

Monolithic metal-organic frameworks for carbon dioxide separation

David G. Madden,[a†] Robin Babu,[a†] Ceren Çamur,[a] Nakul Rampal,[a] Joaquin Silvestre-Albero[b], Teresa Curtin[c] and David Fairen-Jimenez[a*]

[a]Adsorption & Advanced Materials Laboratory (A^{2}ML), Department of Chemical Engineering & Biotechnology, University of Cambridge, Philippa Fawcett Drive, Cambridge, CB3 0AS, United Kingdom

[b]Laboratorio de Materiales Avanzados, Depto. de Química Inorgánica, Universidad de Alicante, E-03690, San Vicente del Raspeig, Spain

[c]Bernal Institute, Department of Chemical Sciences, University of Limerick, Limerick V94 T9PX, Republic of Ireland

[†]These authors contributed equally

[*]e-mail: David Fairen-Jimenez, df334@cam.ac.uk

Table of Contents

Materials & methodology

***mono*HKUST-1 Synthesis.** *mono*HKUST-1 was synthesised using the previously reported method.[1] In a typical synthesis, 6.42 mmol of 1,3,5-benzentricarboxylic acid (H_3BTC) (1.35 g) and 6.42 mmol of $Cu(NO_3)_2{\cdot}2.5H_2O$ (1.5 g) were mixed separately in 100 mL ethanol, and sonicated in an ultrasonic bath for 10 minutes until the solids are completely dissolved. After dissolving the solutions separately, $Cu(NO_3)_2{\cdot}2.5H_2O$ was added to trimesic acid and stirred well at room temperature for 10 min. The reacted solution is then transferred to a falcon tube, centrifuged, and washed with ethanol for 10 minutes (3 × 25 ml, 4200 rpm). After last centrifugation, the supernatant was slowly poured, and the samples are dried overnight to form the *mono*HKUST-1. Activation was carried out by heating to 120 °C under vacuum overnight.

***mono*UiO-66 & *mono*UiO-66-NH_2 Synthesis.** *mono*UiO-66 and *mono*UiO-66-NH_2 were synthesised using the previously reported methods.[2] In a typical *mono*UiO-66 synthesis, 7.25 mmol of benzene-1,4-dicarboxylic acid (H_2BDC) (1.20 g) and 5.0 mmol of zirconium(IV) oxychloride octahydrate (1.61 g) were dissolved in 30 ml of N,N-dimethylformamide (DMF). In a *mono*UiO-66-NH_2 synthesis, H_2BDC is substituted with 2-aminoterephthalic acid (H_2N-H_2BDC). 1.5 mL of concentrated hydrochloric acid (37 %) and 2.0 ml of glacial acetic acid were added to the above solution with strong stirring. The resulting solution was sealed in a 100 mL Pyrex Schott bottle and heated to 100 °C for 2 h. 50 ml of DMF was added to the MOF gel and vigorously mixed. The diluted suspension (7.5 mL per tube) was centrifuged (5 min, 4750 rpm) and the supernatant decanted. The gel was washed again with DMF, centrifuged (4750 rpm) and dried to produce monolithic materials. The obtained monoliths were soaked in acetone (3 × 5 ml, 24 h) and methanol (3 × 5 ml, 24 h) and then dried at room temperature overnight. Final materials were activated by heating to 120 °C under vacuum overnight.

HKUST-1 Synthesis. HKUST-1 was synthesized following previously published procedure.[3] In a typical reaction, 1.00 g (4.76 mmol) of H_3BTC and 2.00 g (6.87 mmol) of $Cu(NO_3)_2{\cdot}3H_2O$ were

mixed and suspended in 20 mL DMF followed by stirring and sonication for 10 minutes. Ethanol (20 mL) was added to this suspension followed by additional stirring and sonication. Finally, deionised water (20 mL) was added to the suspension and the mixture was stirred and sonicated for 30 minutes to allow for complete dissolution of all components. The mixture was heated at 85 ˚C for 24 hours, whereupon blue crystals were obtained, separated *via* filtration, washed and immersed in methanol. The methanol solvent was exchanged twice a day for three days. Final materials were activated by heating to 180 °C under vacuum overnight.

UiO-66 Synthesis. UiO-66 was synthesized following previously published procedure.[4] It was synthesized by dissolving $ZrCl_4$ (0.053 g, 0.227 mmol) and H_2BDC (0.034g, 0.227 mmol) in DMF (24.9 g, 340 mmol) at room temperature. The thus obtained mixture was sealed in a Teflon vessel and placed in a pre-heated oven at 120 ˚C for 24 hours. Crystallization was carried out under static conditions. After cooling in air to room temperature the resulting solid was filtered, washed 3x times with DMF and dried at room temperature. The obtained UiO-66 was soaked in acetonitrile and the solvent was exchanged twice a day for three days before the UiO-66 sample was used for sorption experiments. Final materials were activated by heating to 150 °C under vacuum overnight.

UiO-66-NH_2 Synthesis. UiO-66-NH_2 was synthesized following previously published procedure.[5] A standard upscaled synthesis of UiO-66-NH_2 was performed by dissolving $ZrCl_4$ (1.50 g, 6.4 mmol) and H_2N-H_2BDC (1.56 g, 6.4 mmol) in DMF (180 mL) at room temperature in a volumetric flask. The resulting mixture was placed in a preheated oven at 80 °C for 12 h and then held at 100 °C for 24 h. After the solution was cooled to room temperature in air, the resulting solid was filtered and repeatedly washed with absolute ethanol for 3 days while heated at 60 °C in a water bath. The resulting yellow powder was filtered, transferred to a Schlenk flask, and dried under vacuum at ambient temperature. Final materials were activated by heating to 150 °C under vacuum overnight.

Powder X-ray diffraction (PXRD) patterns were recorded with a Bruker D8 diffractometer at 40 kV and 40 mA using $CuK_{\alpha 1}$ (λ = 1.5405 Å) radiation with a step of 0.02° at a scanning speed of 8 s

per step. Monolith powders were prepared for PXRD analysis by gently crushing with a pestle and mortar before being placed on a zero-background silicon wafer.

Thermogravimetric analysis (TGA) was recorded under nitrogen using TGA instrument TA Q50. Platinum pans and a flow rate of 60 mL min^{-1} for the nitrogen gas were used for the experiments. The data was collected at a temperature ramp of 10 °C min^{-1} up to 700 °C.

Mercury porosimetry was obtained up to a final pressure of 2,000 bar using an AutoPore IV 9500 instrument from Micromeritics. This technique was used to estimate the particle density of both powders and monoliths at atmospheric pressure. Prior to the analysis, all samples were activated overnight at 120 °C (vacuum) before measuring the mass, and then degassed in situ thoroughly before the mercury porosimetry.

Gas adorption measurements. Ultra-high-purity grade CH_4, N_2 and CO_2 were used for gas sorption experiments. Adsorption experiments (up to 1 bar) for different pure gases were performed on Micromeritics 3Flex surface area and pore size analyzer. About 200 mg of activated samples were used for the measurements. A Julabo temperature controller was used to maintain a constant temperature in the bath through the duration of the experiment. Samples were degassed on a Smart VacPrep instrument prior to the analysis.

Isosteric heat of adsorption (Q_{st}) calculations. A virial-type expression of the form below was used to fit the combined isotherm data for all the compounds at 273 and 298 K, where P is the pressure described in Pa, N is the adsorbed amount in mmol/g, T is the temperature in K, a_i and b_i are virial coefficients, and m and n are the number of coefficients used to describe the isotherms. Q_{st} is the coverage-dependent enthalpy of adsorption and R is the universal gas constant. All the related fitting curves are shown in Figure S14-Figure S16.

$$\ln P = \ln N + \sum_{i=0}^{m} a_i N^i + \sum_{i=0}^{n} \binom{n}{k} b_i N^i$$

$$Q_{st} = -R \sum_{i=0}^{m} a_i N^i$$

IAST selectivity calculations. The selectivity for the adsorbate mixture composition of interest were predicted from the single-component adsorption isotherms using Ideal Adsorbed Solution Theory (IAST).[6] First, the single-component isotherms for the adsorbates at 293 K were fitted to the dual-site Langmuir-Freundlich equation (Table S1-S3):

$$n(P) = \frac{n_{m1} b_1 P^{\left(\frac{1}{t_1}\right)}}{1 + b_1 P^{\left(\frac{1}{t_1}\right)}} + \frac{n_{m2} b_2 P^{\left(\frac{1}{t_2}\right)}}{1 + b_2 P^{\left(\frac{1}{t_2}\right)}}$$

In this equation, n is the amount adsorbed per mass of material (in mol/kg), P is the total pressure (in kPa) of the bulk gas at equilibrium with the adsorbed phase, n_{m1} and n_{m2} are the saturation uptakes (in mol/kg) for sites 1 and 2, b_1 and b_2 are the affinity coefficients (in kPa^{-1}) for sites 1 and 2, and t_1 and t_2 represent the deviations from the ideal homogeneous surface (unit-less) for sites 1 and 2. The parameters that were obtained from the fitting for all the three compounds are found in Tables S1–S3, respectively. The final selectivity for adsorbate i relative to adsorbate j was calculated using the following:

$$S_{i/j} = \frac{x_i}{x_j} \frac{y_j}{y_i}$$

Here, x_i and x_j are the mole fractions of components i and j, respectively, in the adsorbed phase, and y_i and y_j are the mole fractions of components i and j, respectively, in the gas phase.

Dynamic mixed gas breakthrough studies. In a typical experiment, *ca.* 0.3 g of pre-activated sample was placed in a quartz tube (Ø = 8 mm) to form a fixed bed held in place using quartz wool. For monolithic samples, individual monoliths were broken and sieved to reduce the particle diameter to *ca.* 2 mm to ensure good packing within the sample tube. Each sample was heated to 353 K under a dry helium flow to remove atmospheric contaminants. Upon cooling, the chosen gas mixture was passed over the packed bed with a total flow rate of 2 $cm^3\ min^{-1}$ at 298 K. The outlet gas concentration

was continuously monitored using an Agilent 5975 MSD mass spectrometer (MS). Upon complete breakthrough and saturation of the packed bed adsorbent, the gas mixed is switched off and dry helium was flowed over the solid. Heating was switch on and samples were heated to 353 K to aid regeneration.

To calculate the CO_2 uptake, initially the gas mixture is passed through an empty reactor containing quartz wool at a flow rate of 2 cm^3 min^{-1} as a blank reference. The gas flow is constantly monitored using the MS. The CO_2 curve is integrated to calculate the area of the curve (A_{Ref}). Upon completion of a CO_2 breakthrough experiment with an adsorbent, the area of the CO_2 adsorption curve is also integrated (A_{Exp}). To calculate the total amount of CO_2 adsorbed, the following equation is used:

$$\text{Total } CO_2 \text{ Uptake} = (A_{Ref} - A_{Exp}) \times CO_2 \text{ flow } (cm^3\ min^{-1})$$

Gravimetric CO_2 uptake experiments. Gravimetric uptakes were recorded using a TA Q50 thermogravimetric analyser (TGA). A flow rate of 20 cm^3 min^{-1} was used for all gases during uptake experiments. Samples were initially heated to 398 K under a 1 bar N_2 flow of 20 cm^3 min^{-1} for 2 h. Once the weight loss stabilises, the sample allowed cool to room temperature before being exposed to a 1 bar CO_2 flow of 20 cm^3 min^{-1}. The weight changes during CO_2 adsorption step were monitored continuously under isothermal condition at 298 K.

Powder X-Ray Diffraction

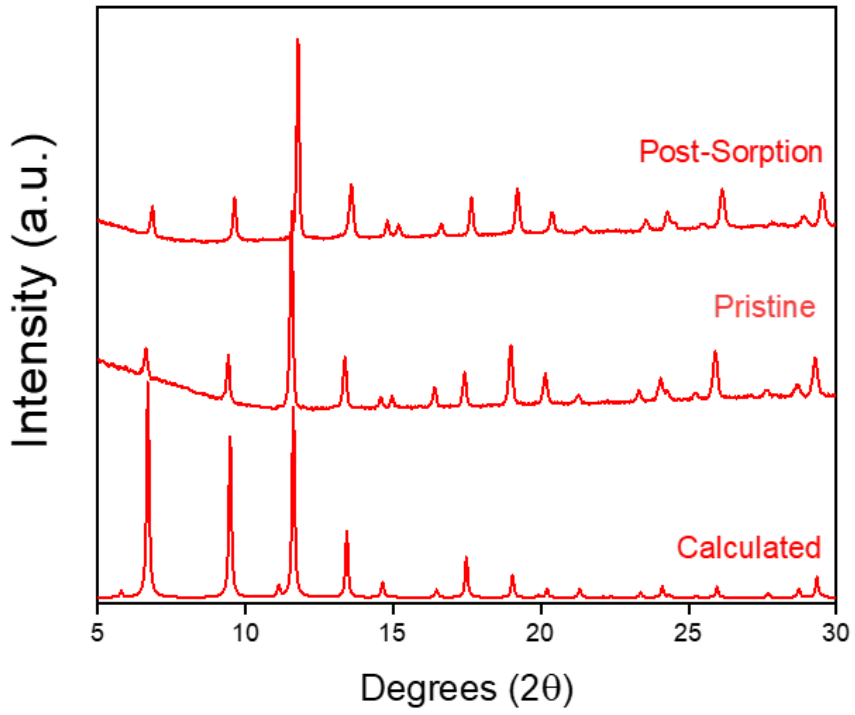

Figure S1: Powder X-ray diffraction patterns for *mono*HKUST-1.

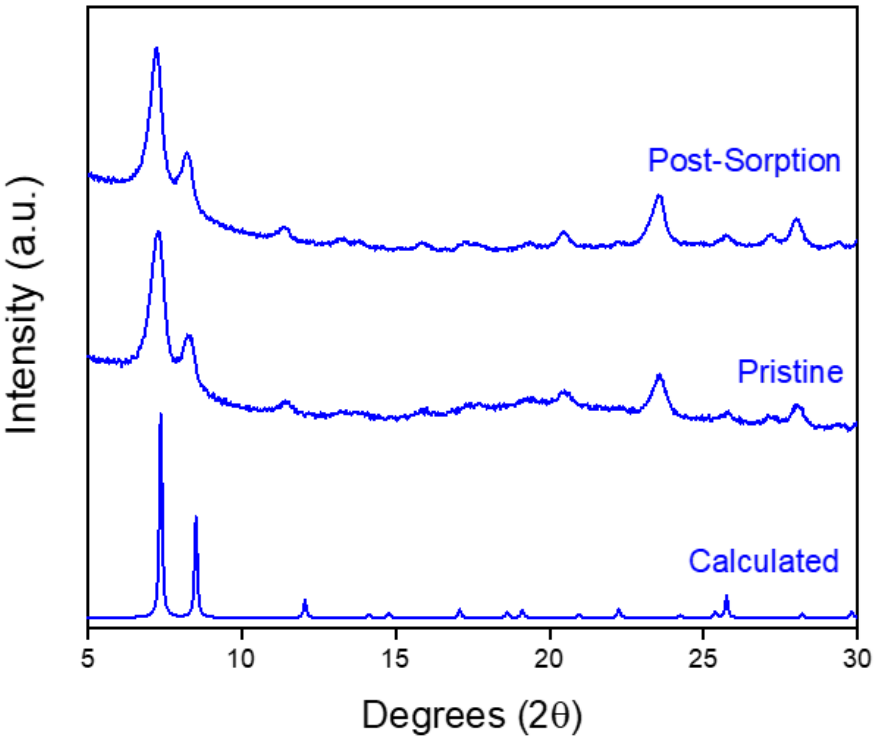

Figure S2: Powder X-ray diffraction patterns for *mono*UiO-66.

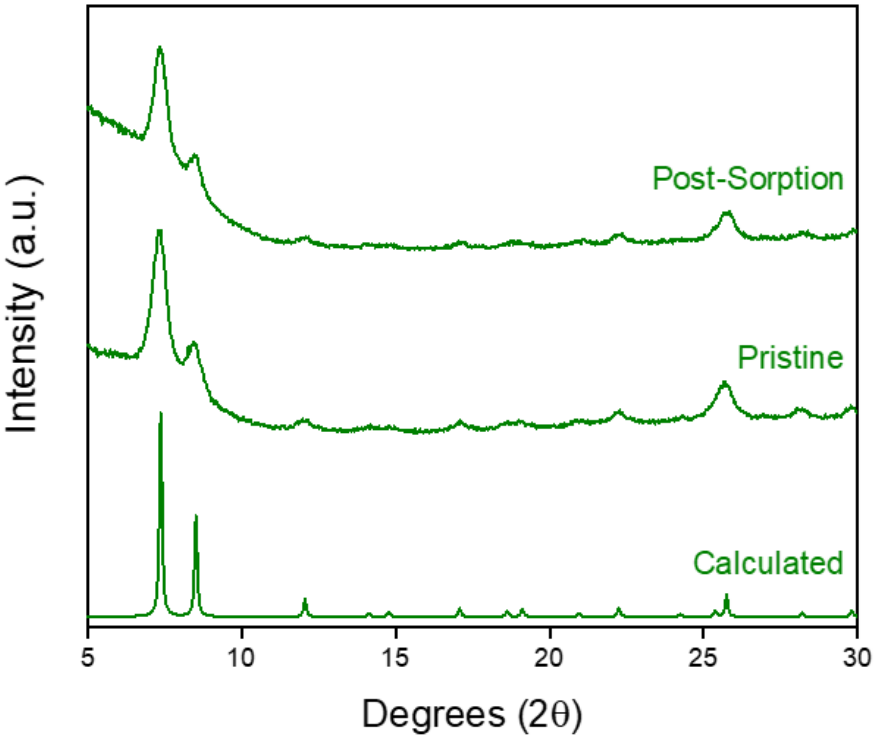

Figure S3: Powder X-ray diffraction patterns for *mono*UiO-66-NH_2.

Thermogravimetric analysis (TGA)

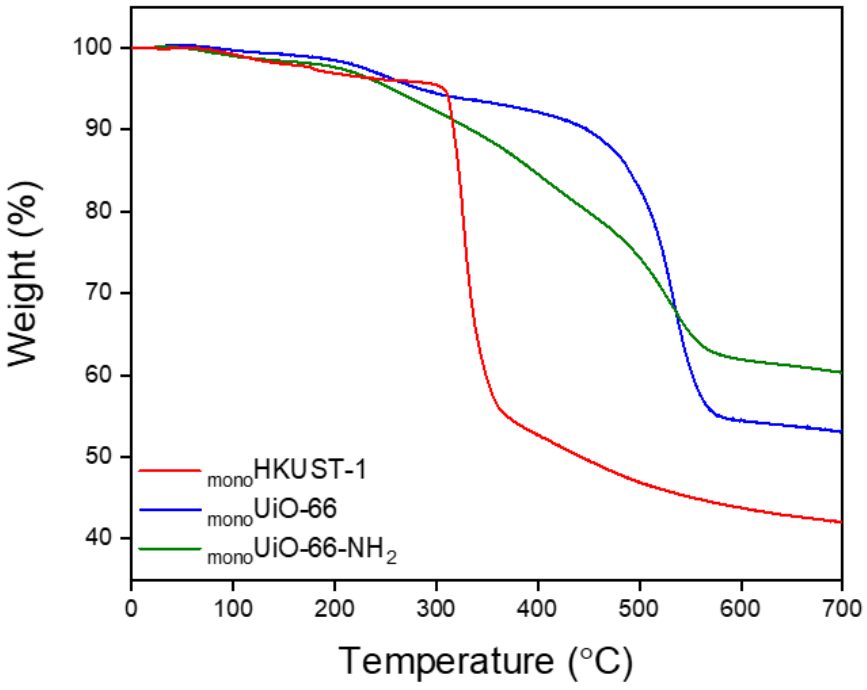

Figure S4: Thermogravimetric analysis for *mono*MOFs.

77 K N_2 adsorption and desorption isotherms

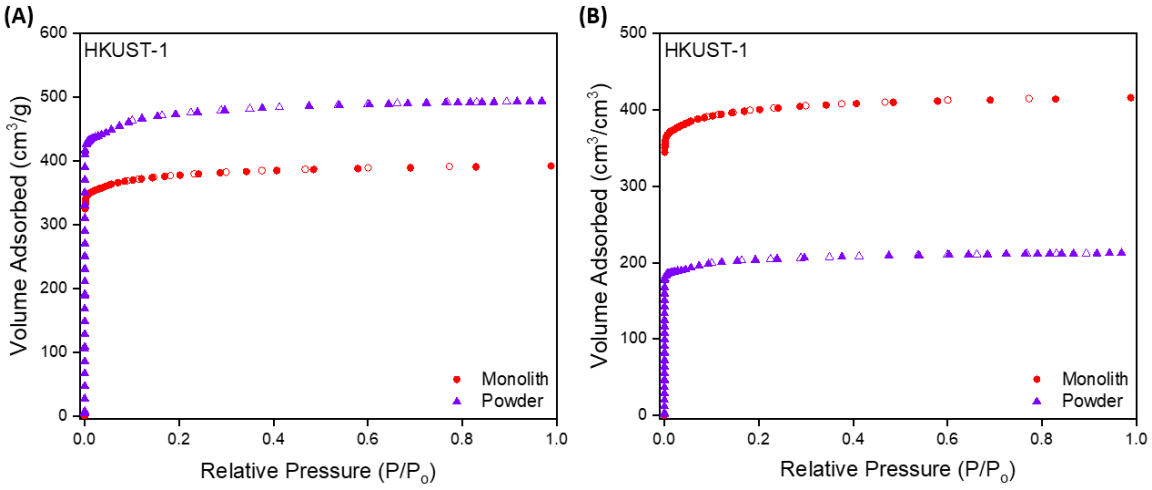

Figure S5: (A) Gravimetric and (B) volumetric 77K N_2 adsorption/desorption isotherms for *mono*HKUST-1.

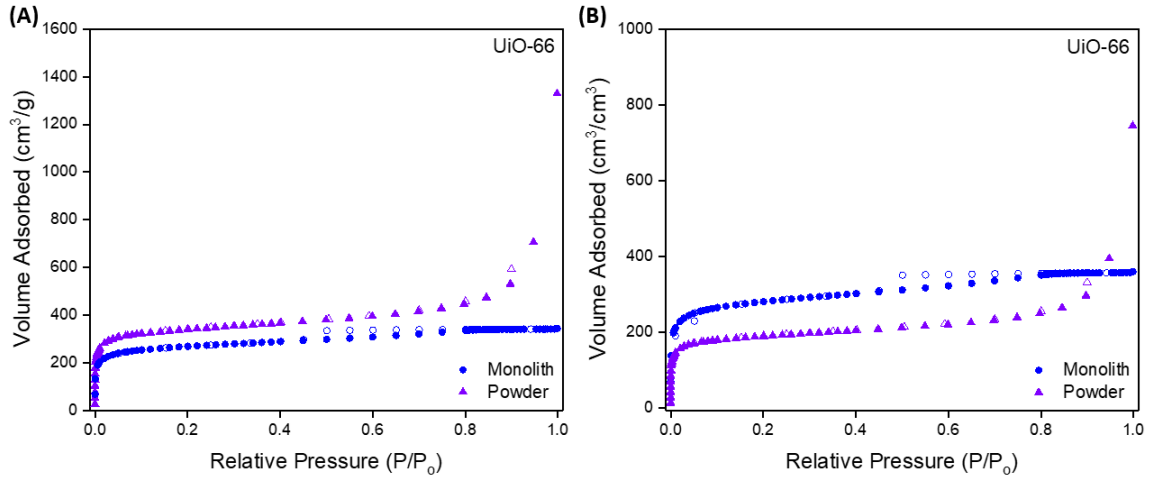

Figure S6: (A) Gravimetric and (B) volumetric 77K N_2 adsorption/desorption isotherms for *mono*UiO-66.

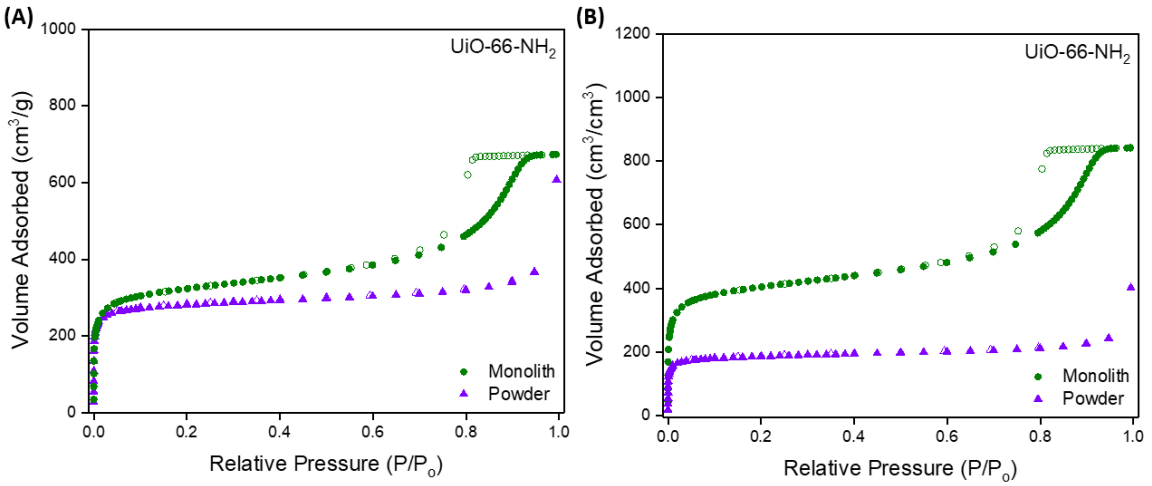

Figure S7: (A) Gravimetric and (B) volumetric 77K N_2 adsorption/desorption isotherms for *mono*UiO-66-NH_2.

BETSI calculated BET areas

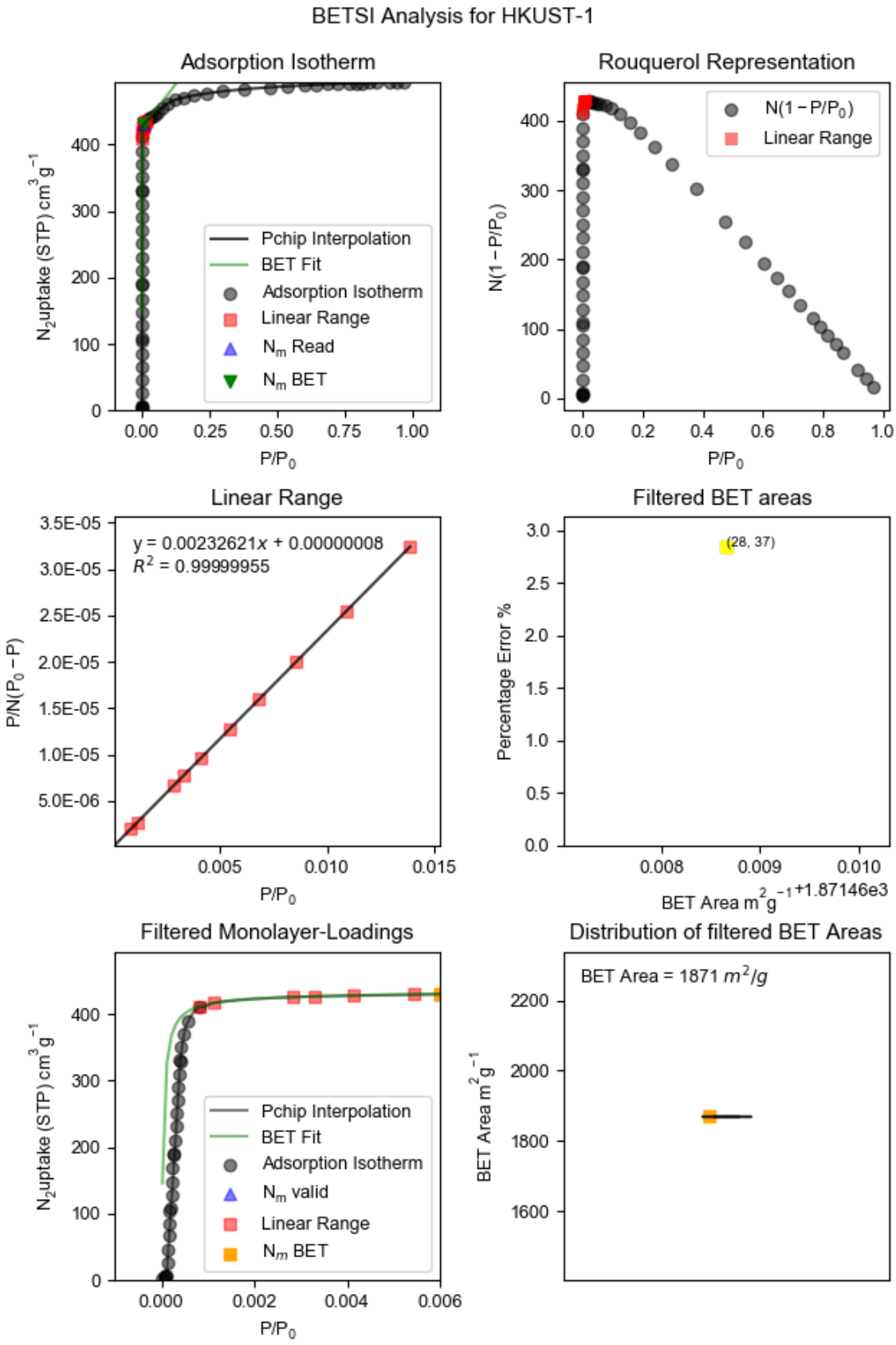

Figure S8: BETSI calculated BET area for HKUST-1.

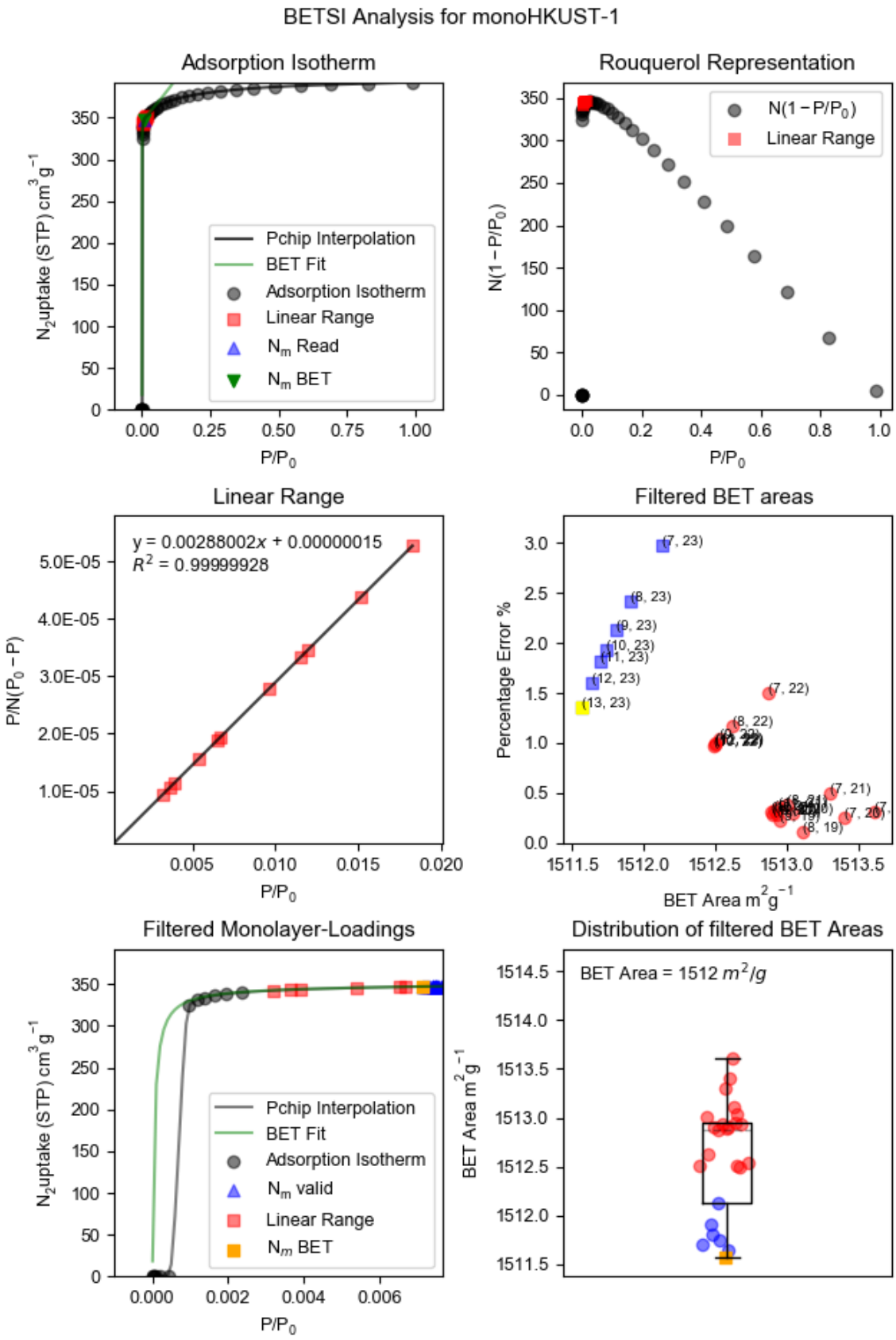

Figure S9: BETSI calculated BET area for *mono*HKUST-1.

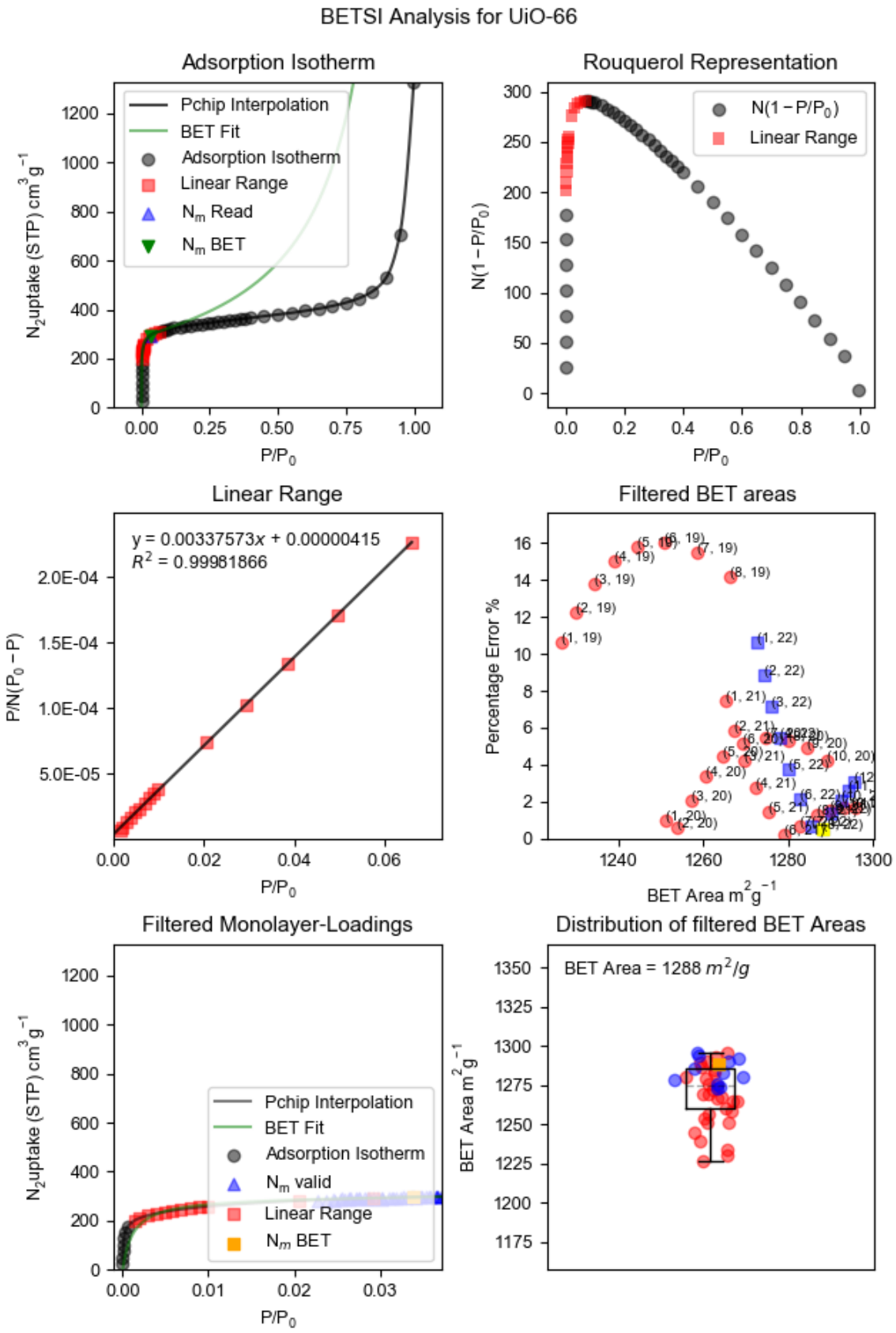

Figure S10: BETSI calculated BET area for UiO-66.

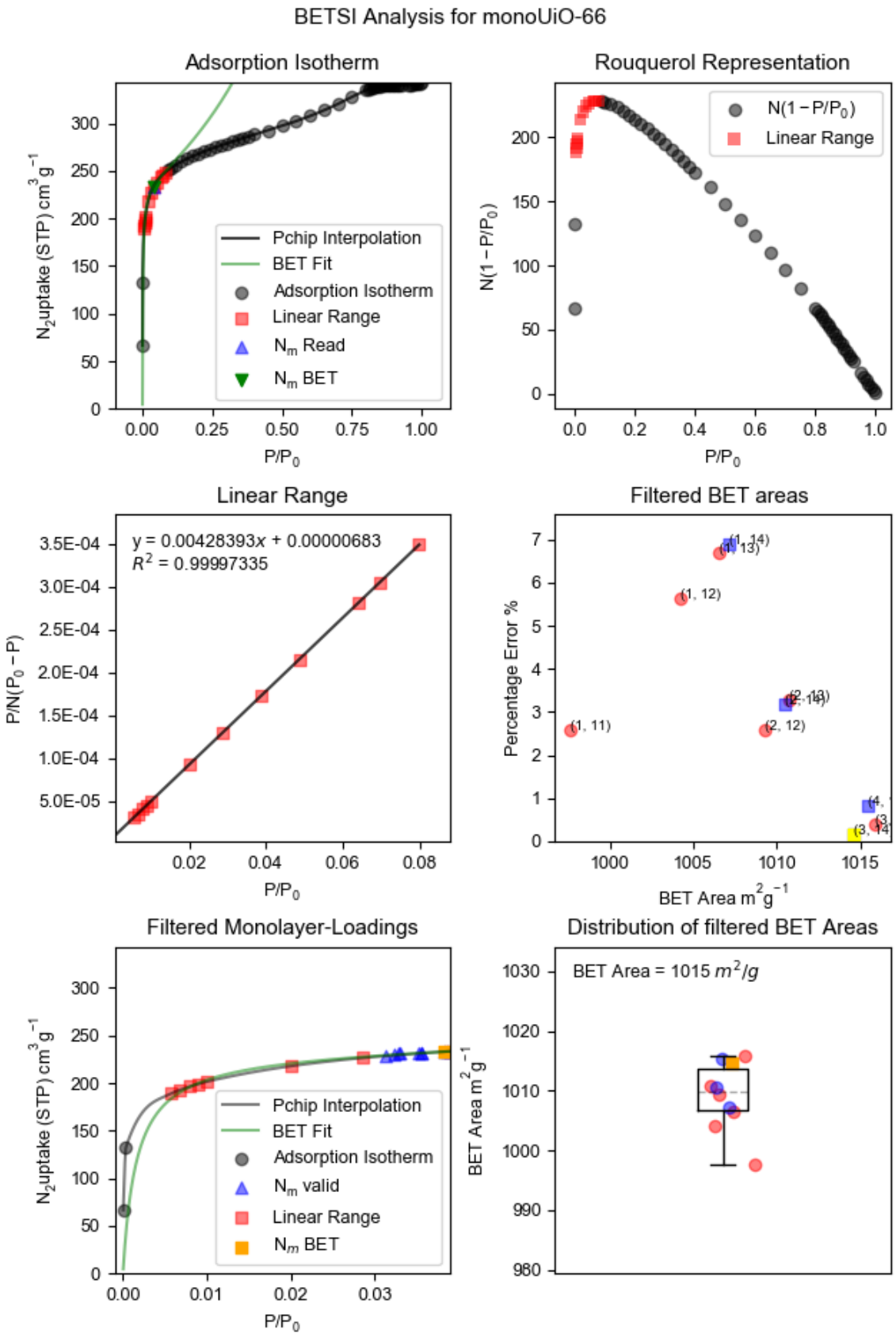

Figure S11: BETSI calculated BET area for *mono*UiO-66.

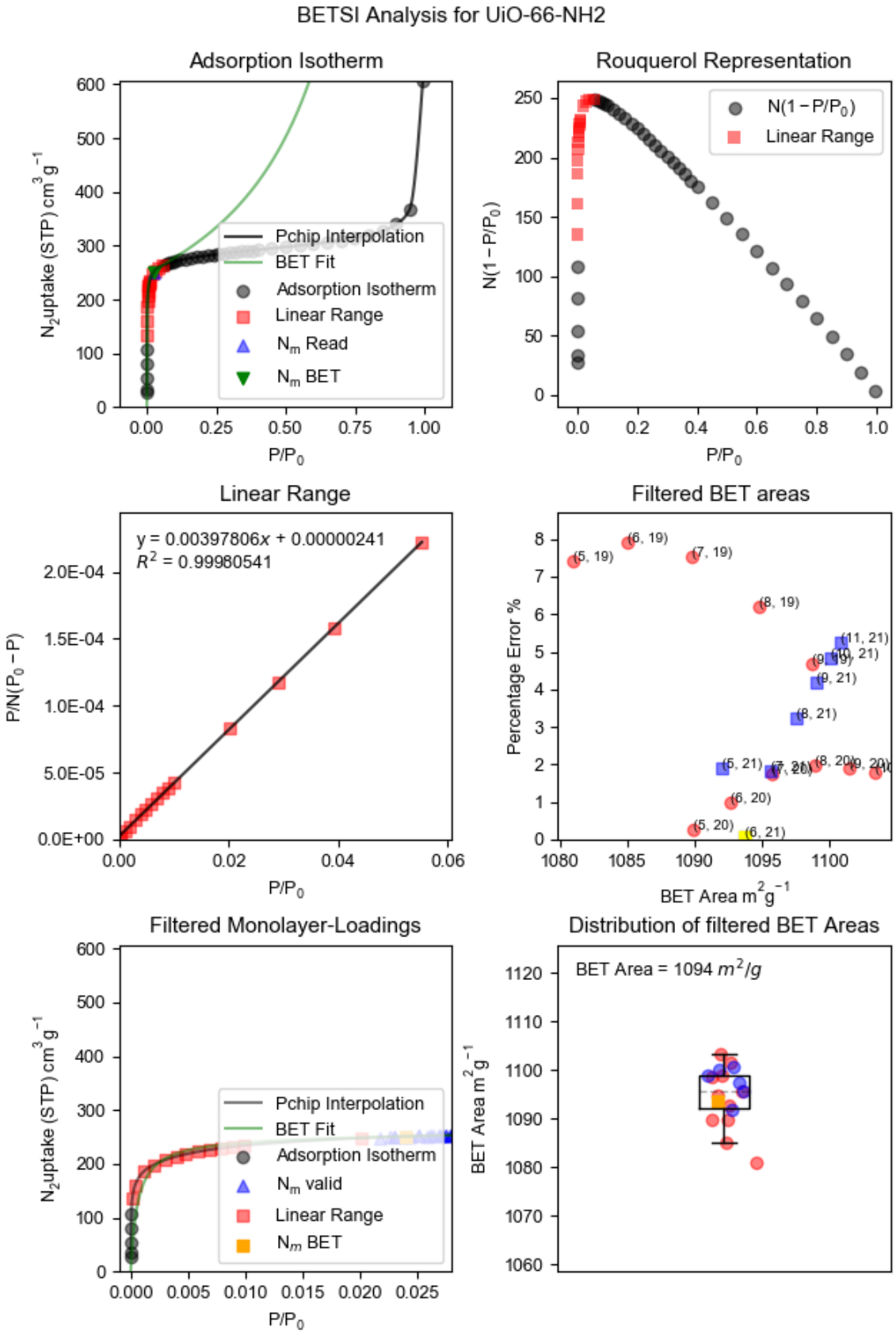

Figure S12: BETSI calculated BET area for UiO-66-NH_2.

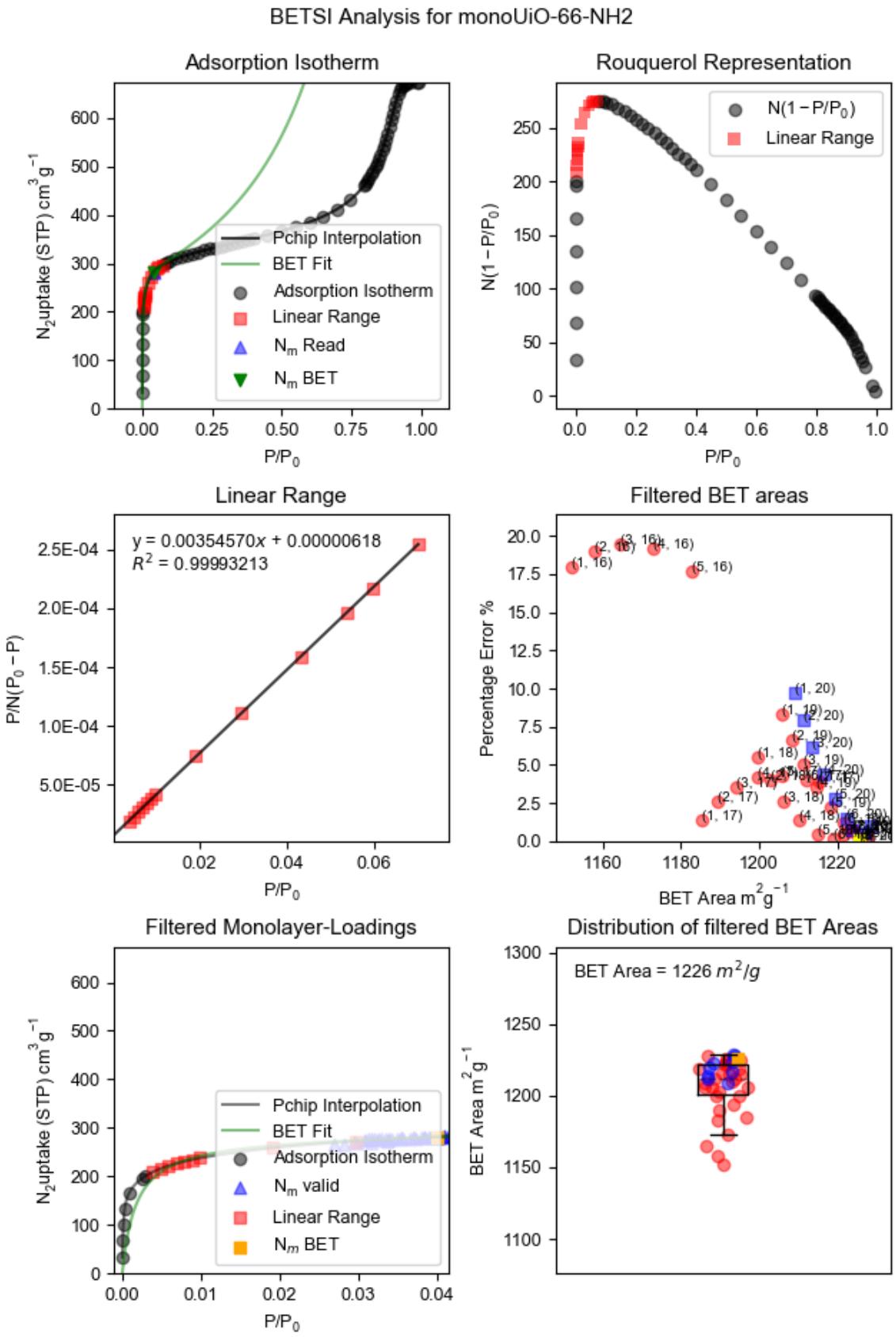

Figure S13: BETSI calculated BET area for *mono*UiO-66-NH_2.

Single-component gas adsorption studies

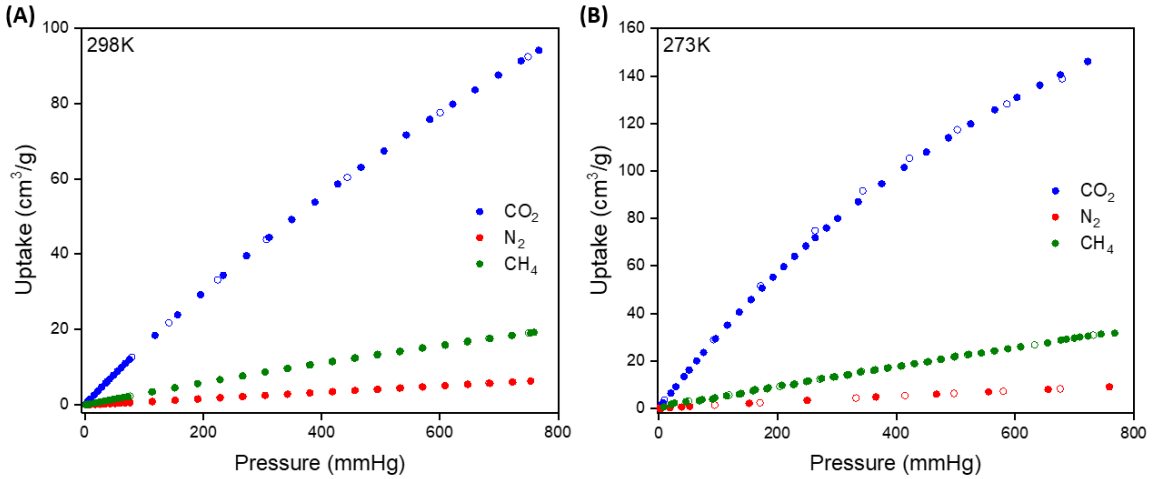

Figure S14: (A) 298K and (B) 273K CO_2, N_2 and CH_4 adsorption/desorption isotherms for *mono*HKUST-1.

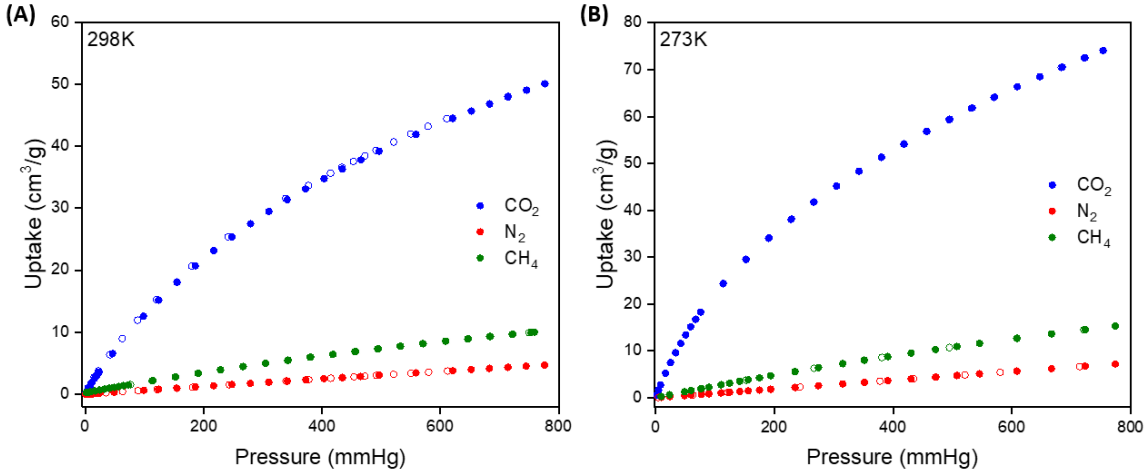

Figure S15: (A) 298K and (B) 273K CO_2, N_2 and CH_4 adsorption/desorption isotherms for *mono*UiO-66.

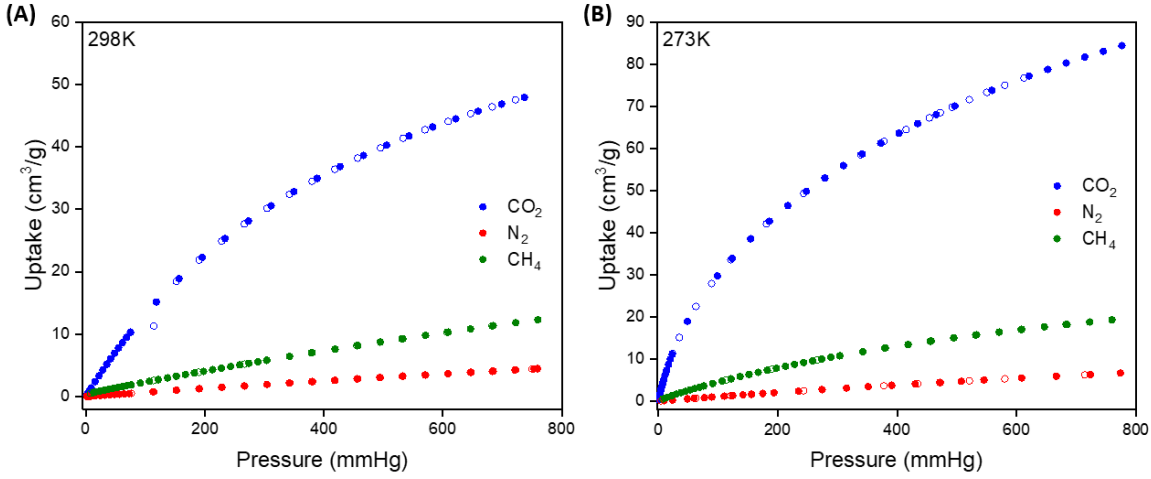

Figure S16: (A) 298K and (B) 273K CO_2, N_2 and CH_4 adsorption/desorption isotherms for *mono*UiO-66-NH_2.

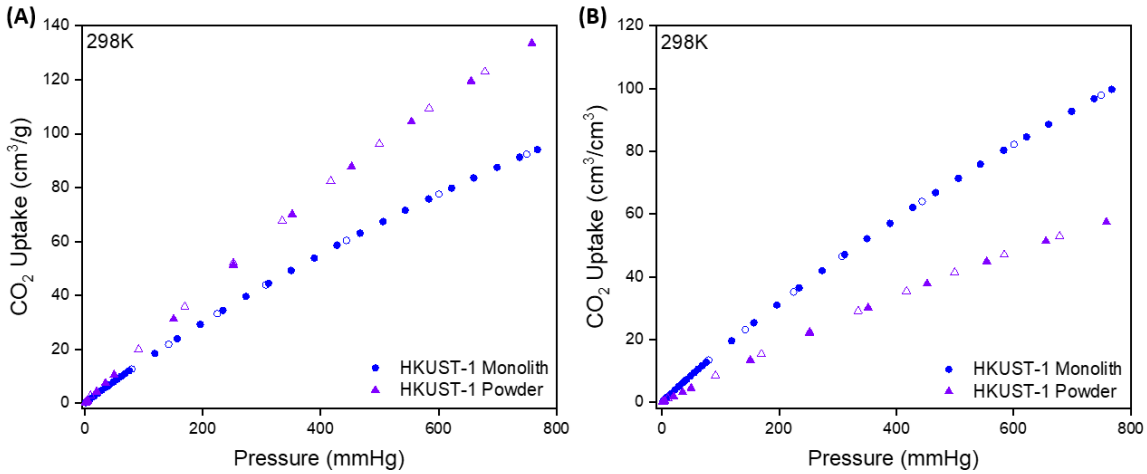

Figure S17: (A) Gravimetric and (B) volumetric 298K CO_2 adsorption/desorption isotherms for *mono*HKUST-1 and powdered HKUST-1.

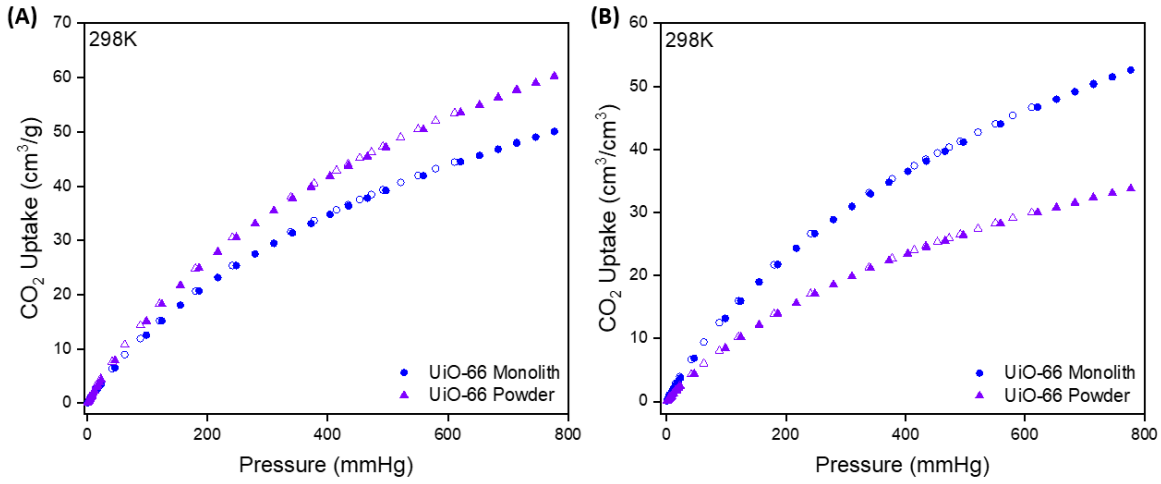

Figure S18: (A) Gravimetric and (B) volumetric 298K CO_2 adsorption/desorption isotherms for *mono*UiO-66 and powdered UiO-66.

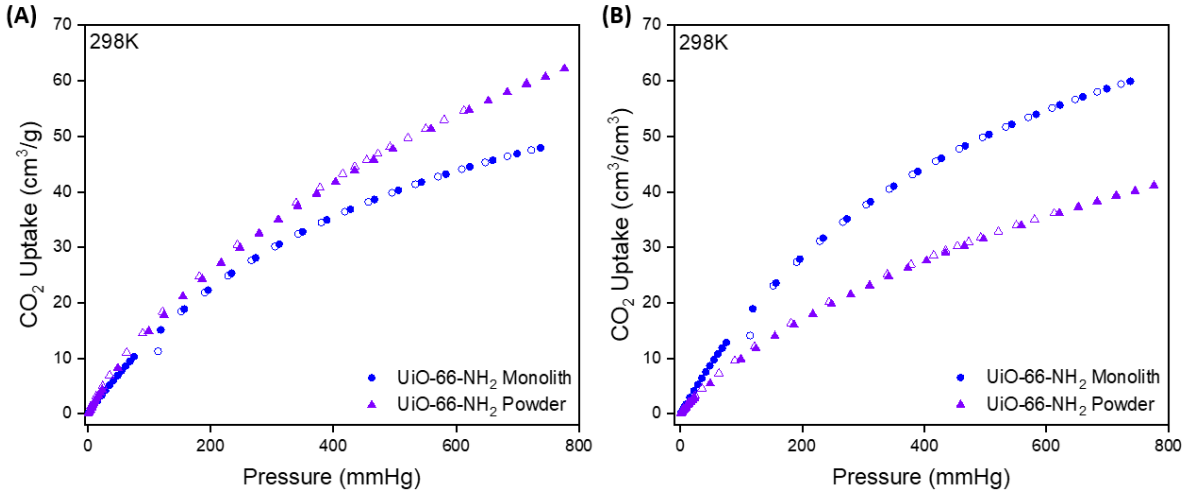

Figure S19: (A) Gravimetric and (B) volumetric 298K CO_2 adsorption/desorption isotherms for *mono*UiO-66-NH_2 and powdered UiO-66-NH_2.

Isosteric heat of adsorption (Q_{st})

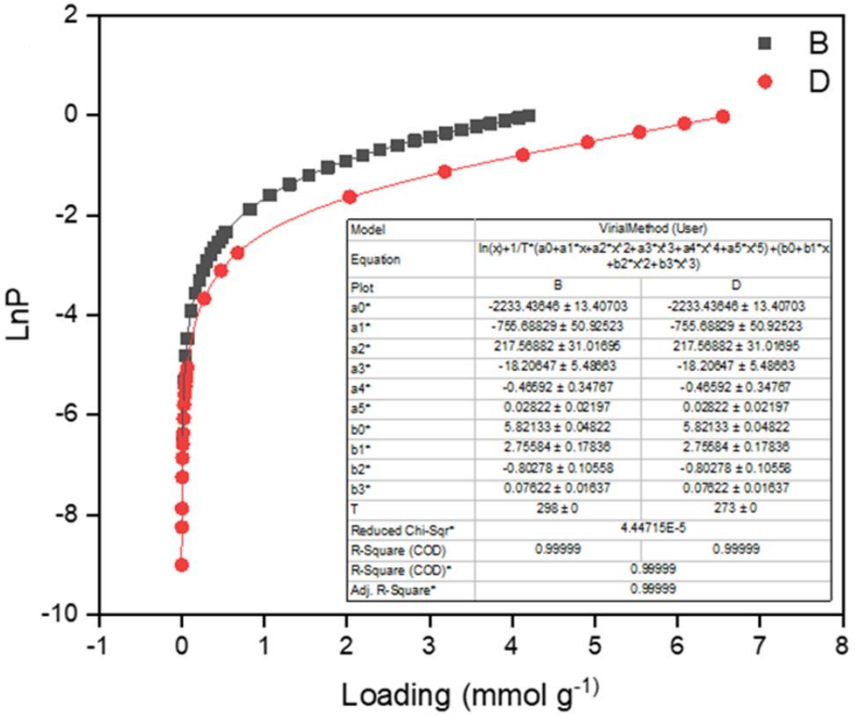

Figure S20: Fitting of the CO_2 adsorption isotherms at 298K and 273K for *mono*HKUST-1 to the virial equation.

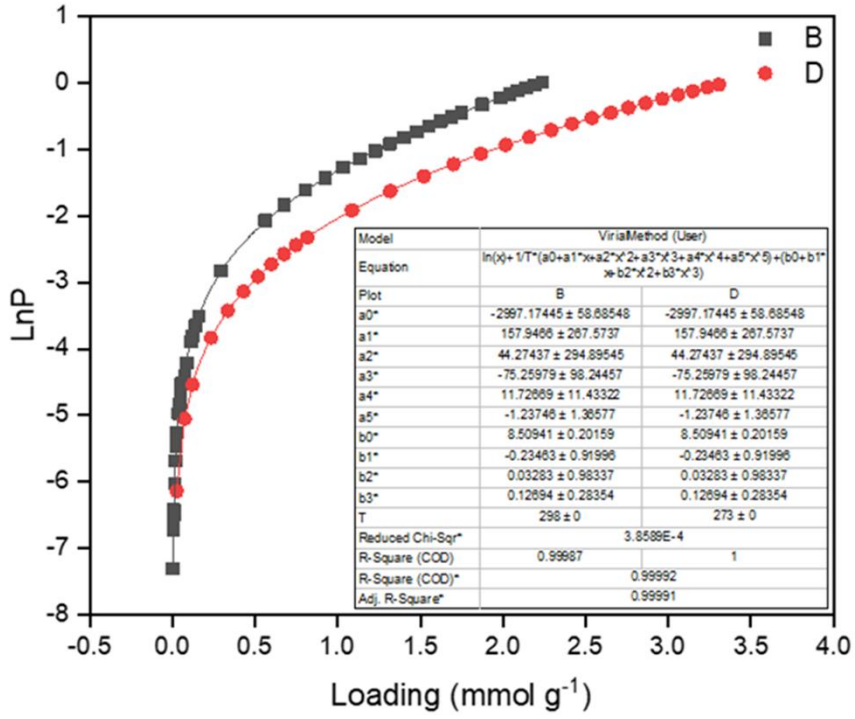

Figure S21: Fitting of the CO_2 adsorption isotherms at 298K and 273K for *mono*UiO-66 to the virial equation.

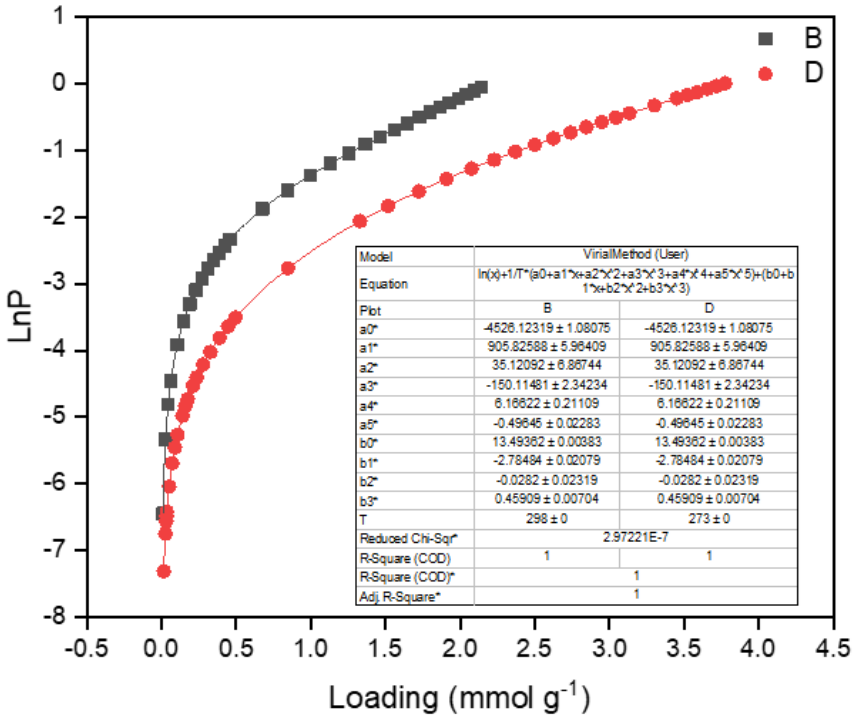

Figure S22: Fitting of the CO_2 adsorption isotherms at 298K and 273K for *mono*UiO-66-NH_2 to the virial equation.

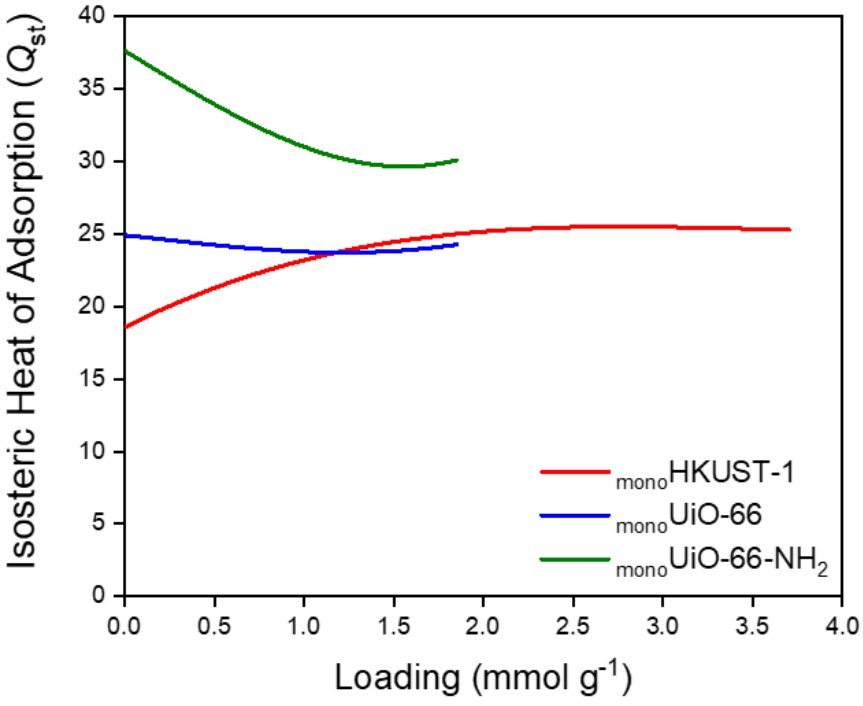

Figure S23: CO_2 isosteric heats of adsorption (Q_{st}) for *mono*HKUST-1, *mono*UiO-66 and *mono*UiO-66-NH_2.

Dual-Site Langmuir-Freundlich Fittings

Table S1: Dual-site Langmuir-Freundlich fitting parameters for CO_2 adsorption at 298 K.

Material	Q_1	Q_2	K_1	K_2	n_1	n_2
*mono*HKUST-1	1.06262	423.291	0.015992	0.000367	0.956619	0.997919
*mono*UiO-66	89.866	2.125E-17	0.0015654	4.0733E-7	0.96962	9.8224E-6
*mono*UiO-66-NH_2	78.6819	3.35458	0.0019191	0.0016692	0.999818	1.00644

Table S2: Dual-site Langmuir-Freundlich fitting parameters for N_2 adsorption at 298 K.

Material	Q_1	Q_2	K_1	K_2	n_1	n_2
*mono*HKUST-1	11.5122	41.6868	0.000784	0.000246	1.04521	1.73888
*mono*UiO-66	60.1968	0.434225	0.00012138	0.0028097	1.0757	0.863726
*mono*UiO-66-NH_2	28.0078	0.366539	0.00025673	0.0030404	1.06076	0.862987

Table S3: Dual-site Langmuir-Freundlich fitting parameters for CH_4 adsorption at 298 K.

Material	Q_1	Q_2	K_1	K_2	n_1	n_2
*mono*HKUST-1	108.51	4.19E-11	0.000276	2.39E-12	0.985486	4.02E-07
*mono*UiO-66	0.456142	33.7456	0.0056682	0.0005371	0.001992	1.00043
*mono*UiO-66-NH_2	0.897495	54.9866	0.0475446	0.00036784	0.246157	1.02974

Ideal Adsorbed Solution Theory (IAST) studies

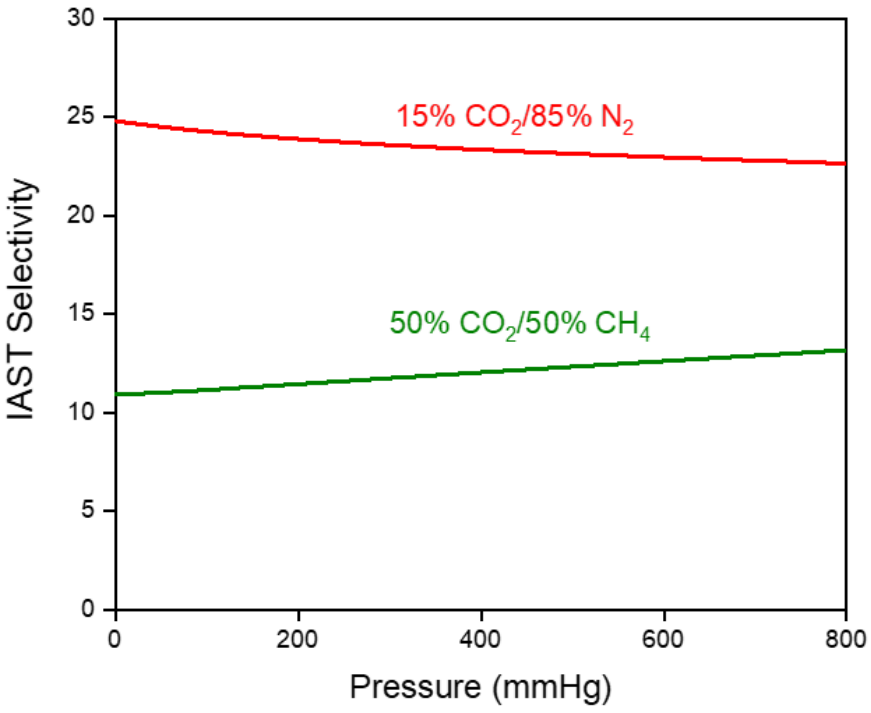

Figure S24: IAST selectivity's for 15% CO_2/85% N_2 and 50% CO_2/50% CH_4 *v/v* gas mixtures for *mono*HKUST-1 at 298K.

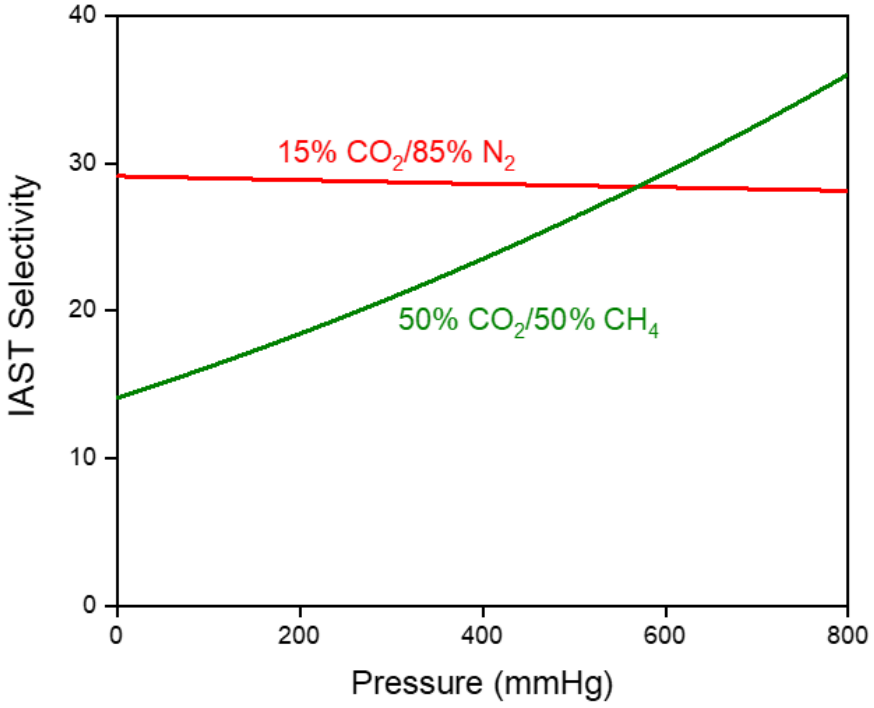

Figure S25: IAST selectivity's for 15% CO_2/85% N_2 and 50% CO_2/50% CH_4 *v/v* gas mixtures for *mono*UiO-66 at 298K.

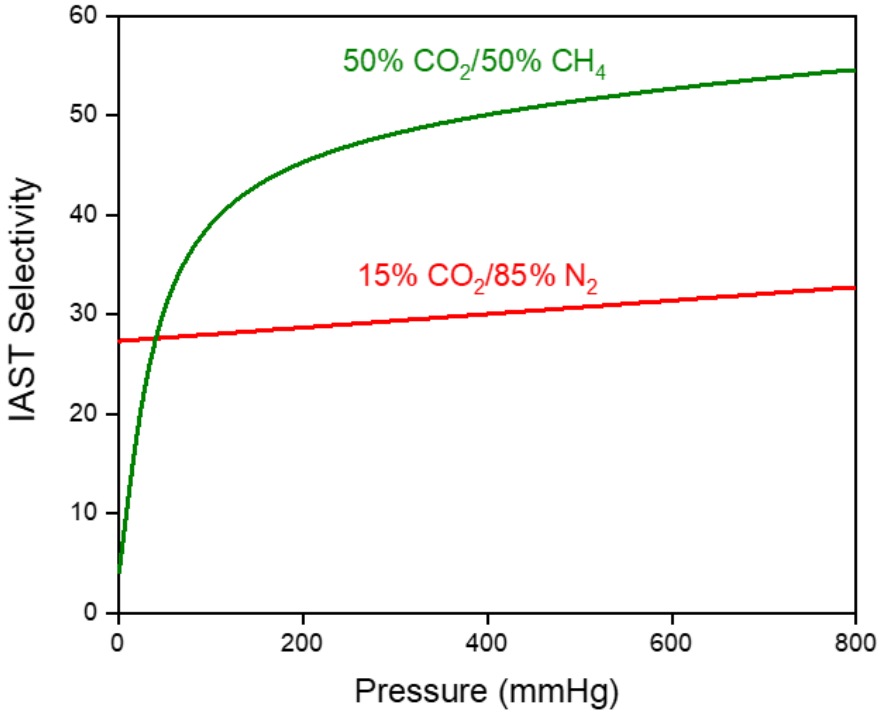

Figure S26: IAST selectivity's for 15% CO_2/85% N_2 and 50% CO_2/50% CH_4 *v/v* gas mixtures for *mono*UiO-66-NH_2 at 298K.

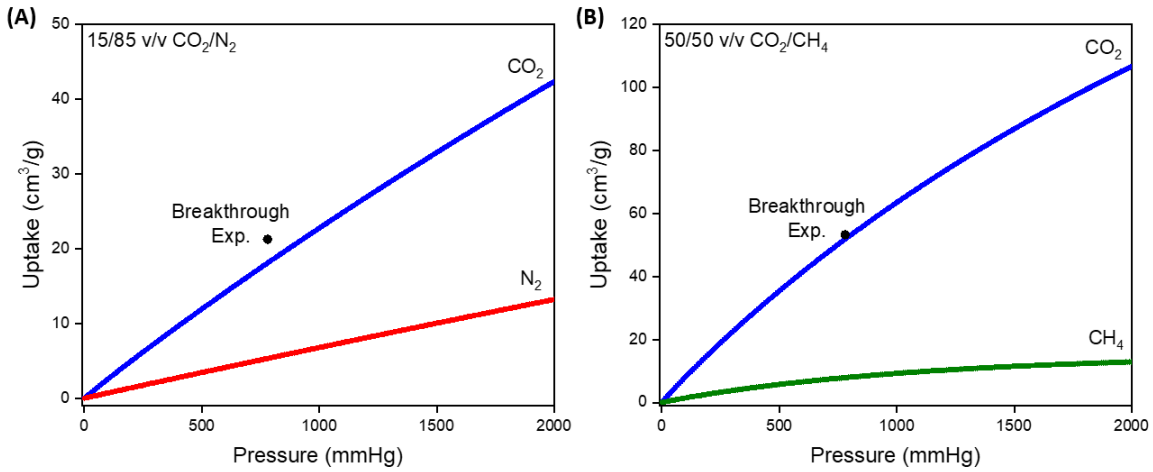

Figure S27: IAST predicted uptakes for (A) 15% CO_2/85% N_2 and (B) 50% CO_2/50% CH_4 *v/v* gas mixtures for *mono*HKUST-1 at 298K with breakthrough results for comparison.

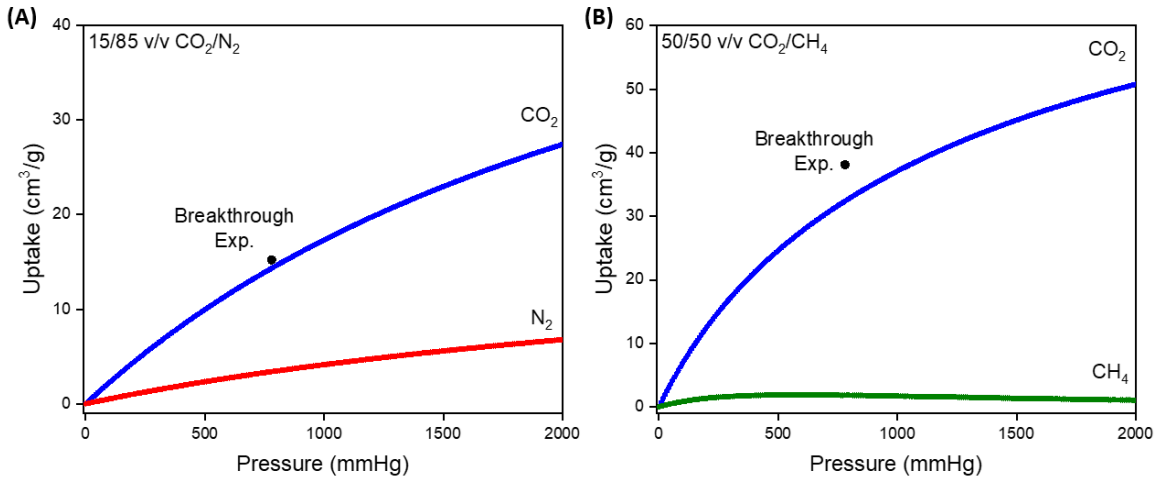

Figure S28: IAST predicted uptakes for (A) 15% CO_2/85% N_2 and (B) 50% CO_2/50% CH_4 *v/v* gas mixtures for *mono*UiO-66 at 298K with breakthrough results for comparison.

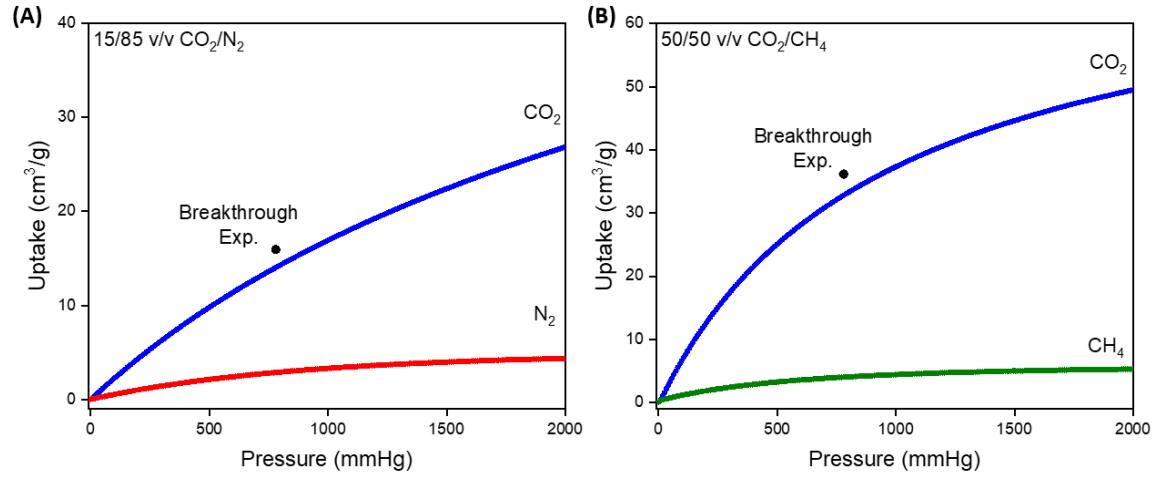

Figure S29: IAST predicted uptakes for (A) 15% CO_2/85% N_2 and (B) 50% CO_2/50% CH_4 *v/v* gas mixtures for *mono*UiO-66-NH_2 at 298K with breakthrough results for comparison.

CO_2 uptake kinetics studies

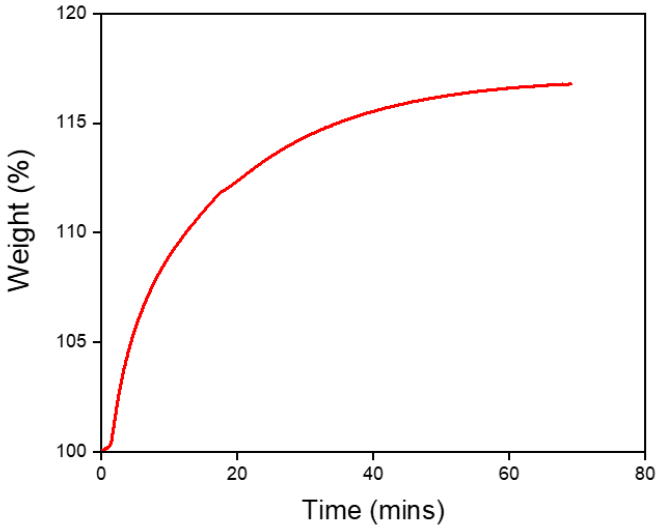

Figure S30: 1.0 bar gravimetric CO_2 uptake versus time for *mono*HKUST-1 at 298 K.

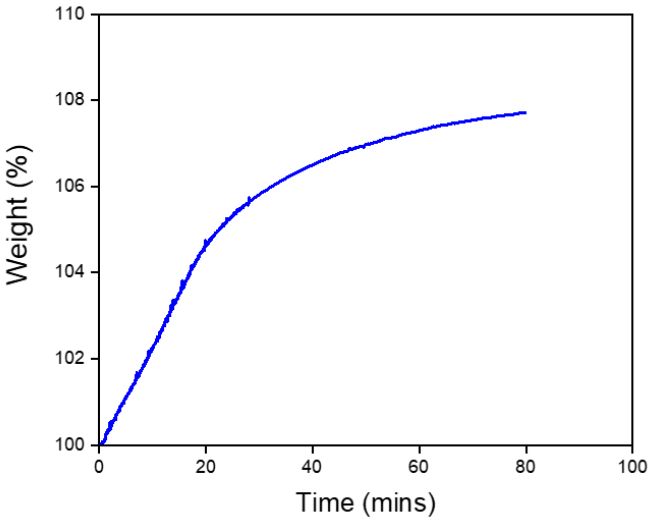

Figure S31: 1.0 bar gravimetric CO_2 uptake versus time for *mono*UiO-66 at 298 K.

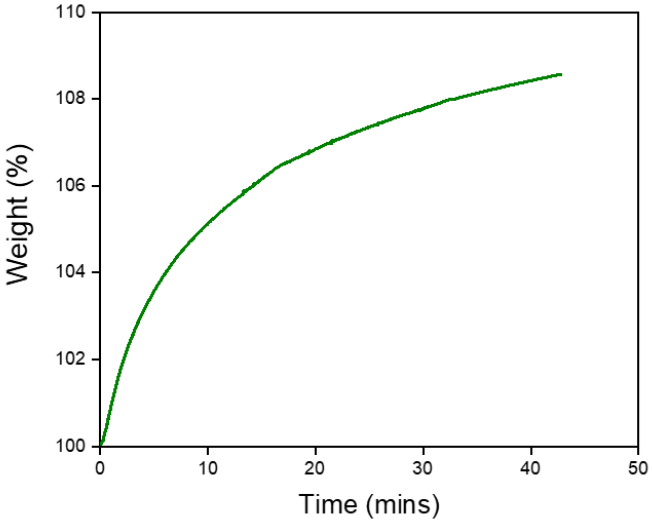

Figure S32: 1.0 bar gravimetric CO_2 uptake versus time for *mono*UiO-66-NH_2 at 298 K.

Dynamic mixed gas breakthrough studies

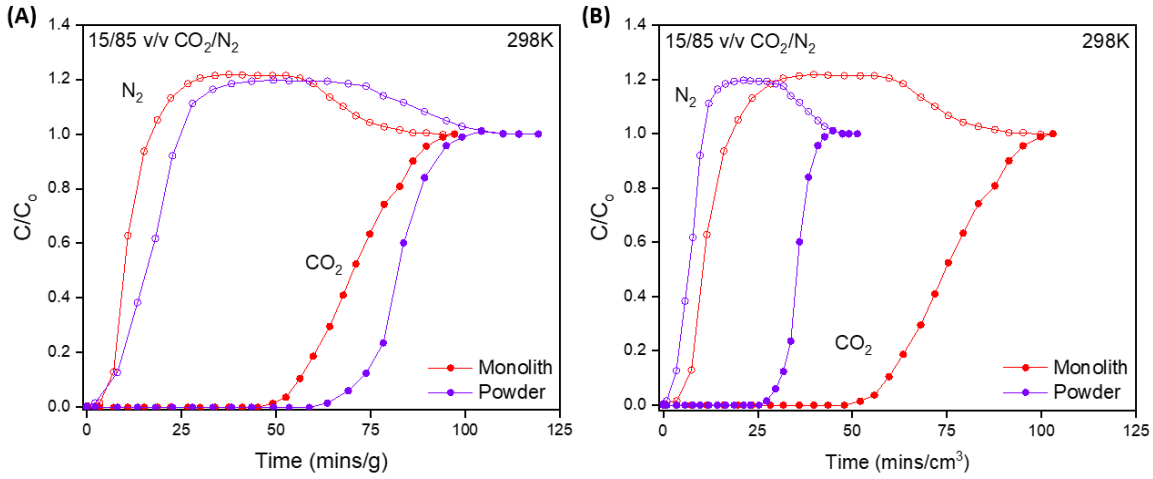

Figure S33: (A) Gravimetric and (B) volumetric 15% CO_2/85% N_2 *v/v* breakthrough studies for powdered HKUST-1 and *mono*HKUST-1 at 298K (Total flow = 2 cm^3 min^{-1}).

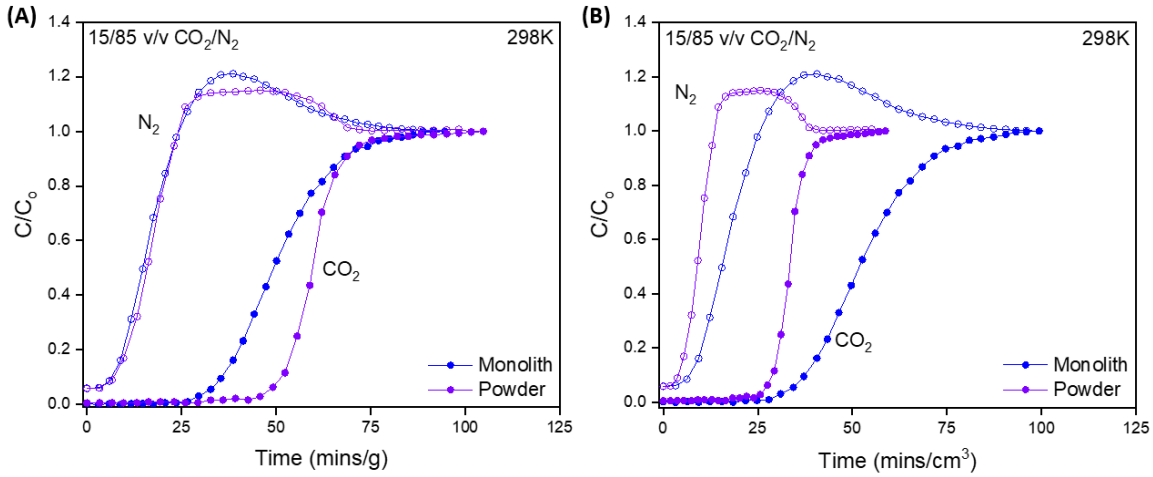

Figure S34: (A) Gravimetric and (B) volumetric 15% CO_2/85% N_2 *v/v* breakthrough studies for powdered UiO-66 and *mono* UiO-66 at 298K (Total flow = 2 cm^3 min^{-1}).

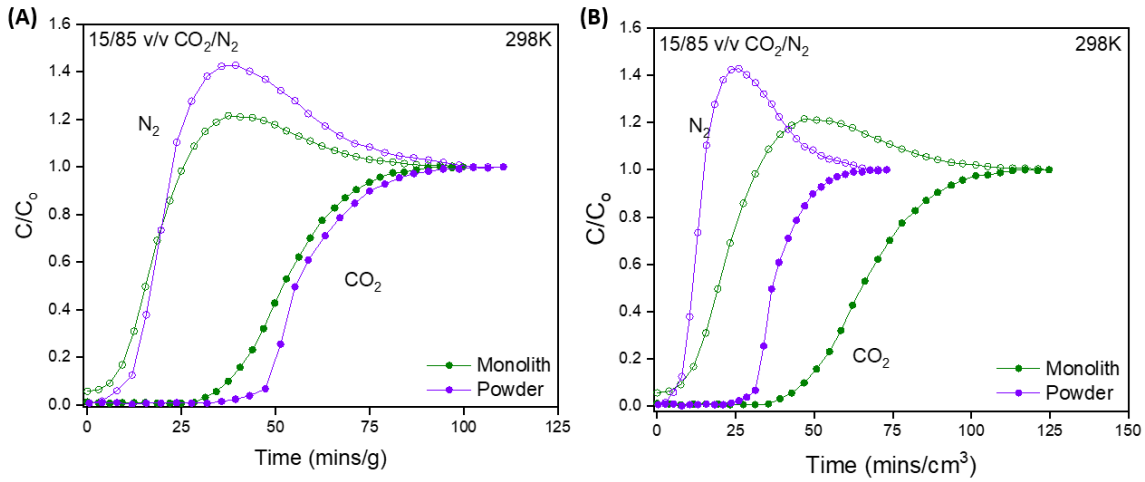

Figure S35: (A) Gravimetric and (B) volumetric 15% CO_2/85% N_2 *v/v* breakthrough studies for powdered UiO-66-NH_2 and *mono* UiO-66-NH_2 at 298K (Total flow = 2 cm^3 min^{-1}).

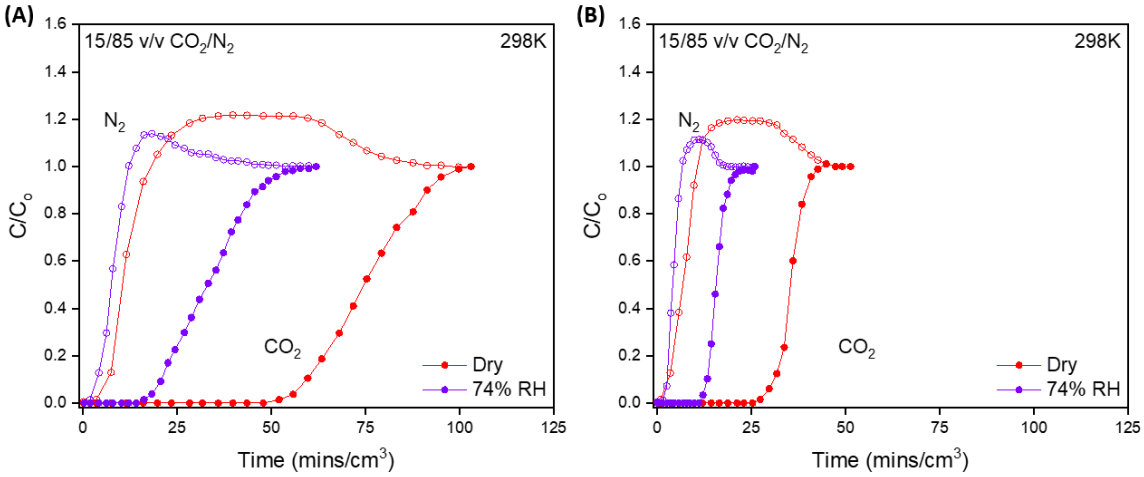

Figure S36: Dry and 74% relative humidity 15% CO_2/85% N_2 *v/v* breakthrough studies for (A) *mono*HKUST-1 and (B) powdered HKUST-1 and at 298K (Total flow = 2 cm^3 min^{-1}).

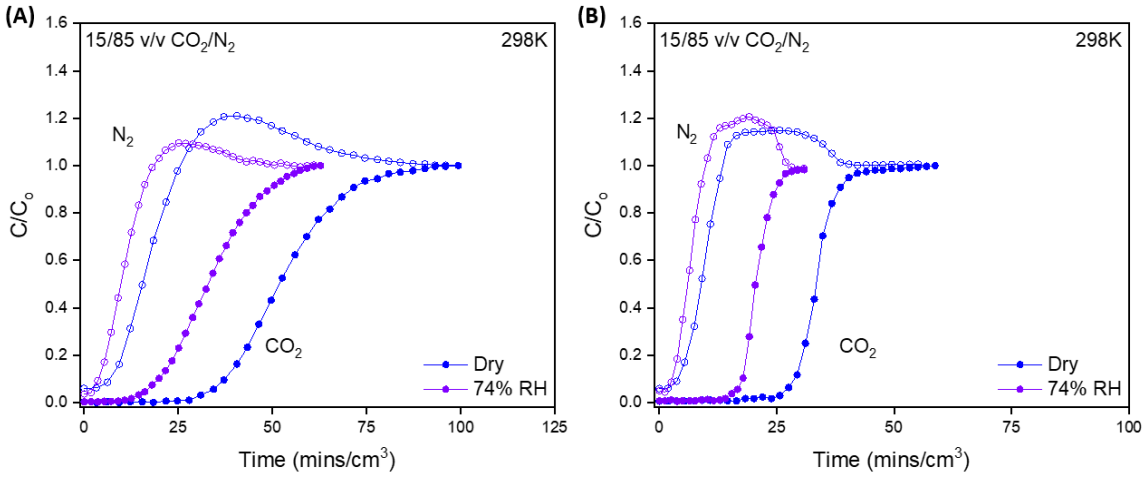

Figure S37: Dry and 74% relative humidity 15% CO_2/85% N_2 *v/v* breakthrough studies for (A) *mono*UiO-66 and (B) powdered UiO-66 and at 298K (Total flow = 2 cm^3 min^{-1}).

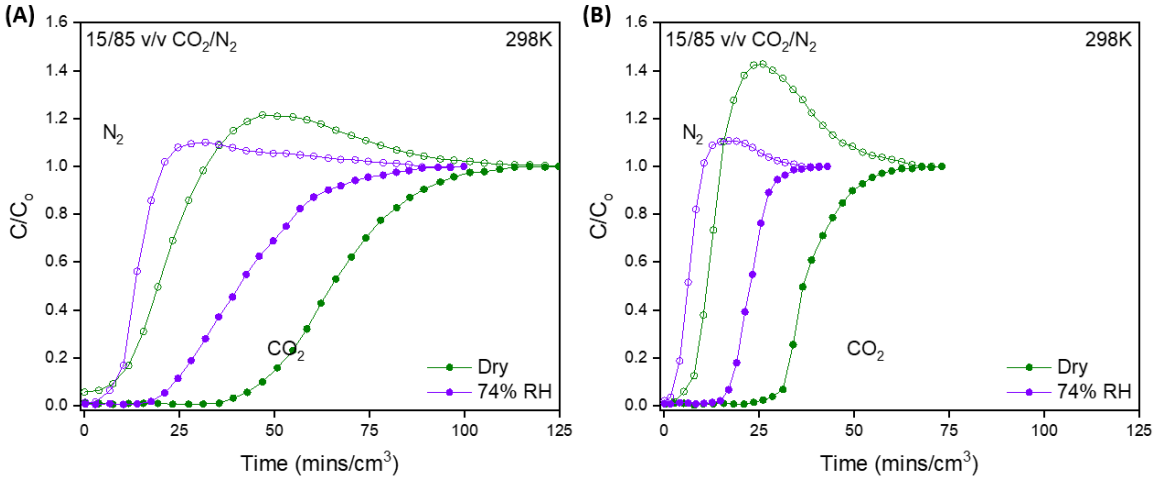

Figure S38: Dry and 74% relative humidity 15% CO_2/85% N_2 *v/v* breakthrough studies for (A) *mono*UiO-66-NH_2 and (B) powdered UiO-66-NH_2 and at 298K (Total flow = 2 cm^3 min^{-1}).

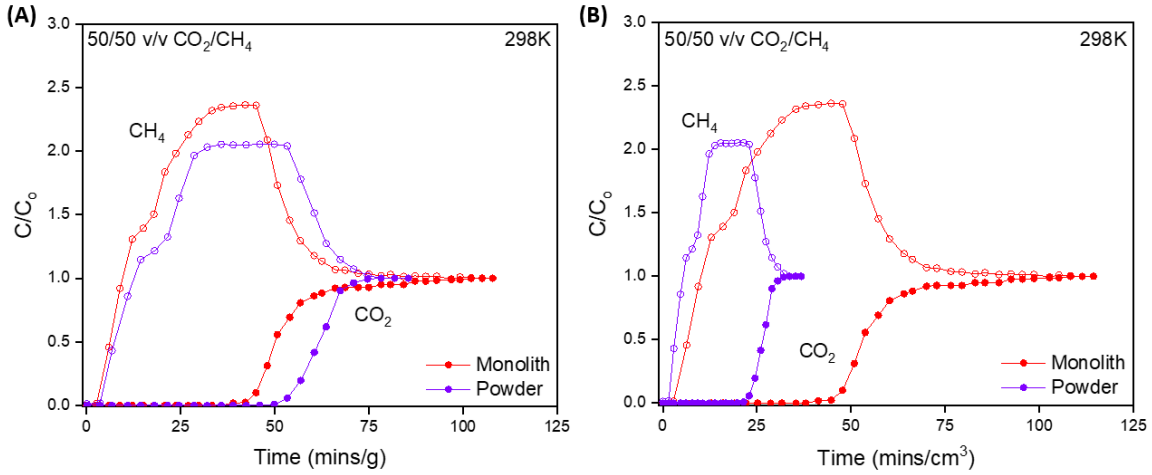

Figure S39: (A) Gravimetric and (B) volumetric 50% CO_2/50% CH_4 *v/v* breakthrough studies for powdered HKUST-1 and *mono*HKUST-1 at 298K (Total flow = 2 cm^3 min^{-1}).

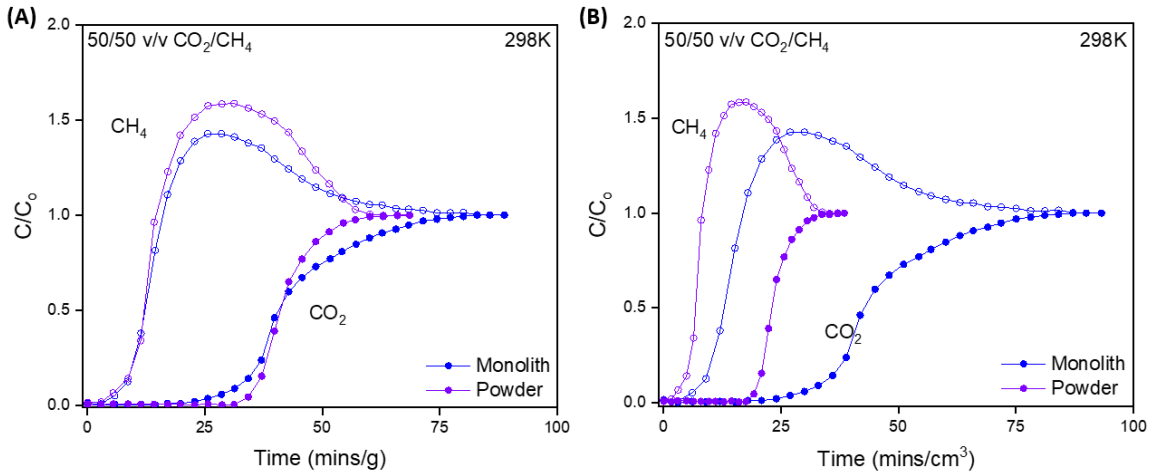

Figure S40: (A) Gravimetric and (B) volumetric 50% CO_2/50% CH_4 *v/v* breakthrough studies for powdered UiO-66 and *mono* UiO-66 at 298K (Total flow = 2 cm^3 min^{-1}).

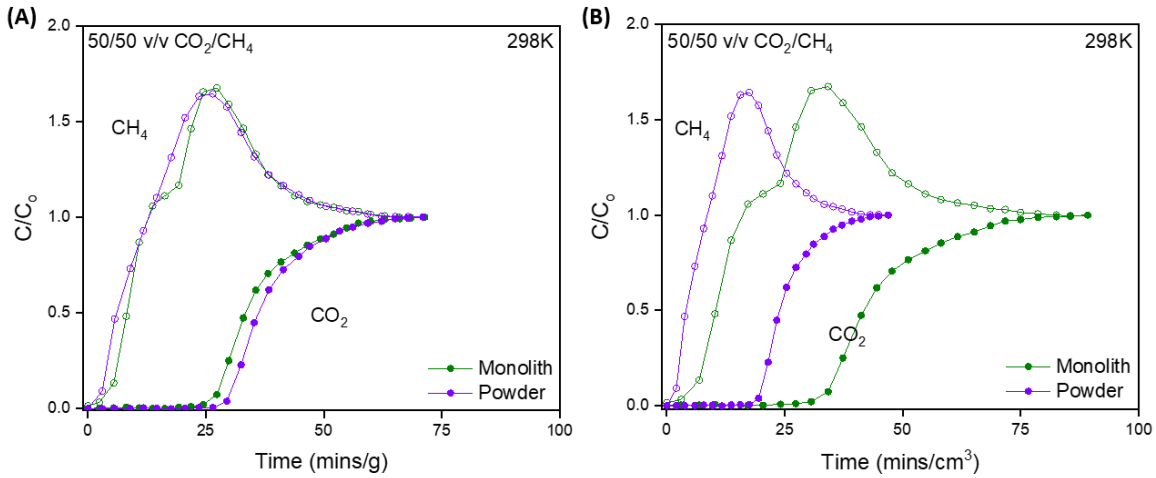

Figure S41: (A) Gravimetric and (B) volumetric 50% CO_2/50% CH_4 *v/v* breakthrough studies for powdered UiO-66-NH_2 and *mono* UiO-66-NH_2 at 298K (Total flow = 2 cm^3 min^{-1}).

Cyclability Testing

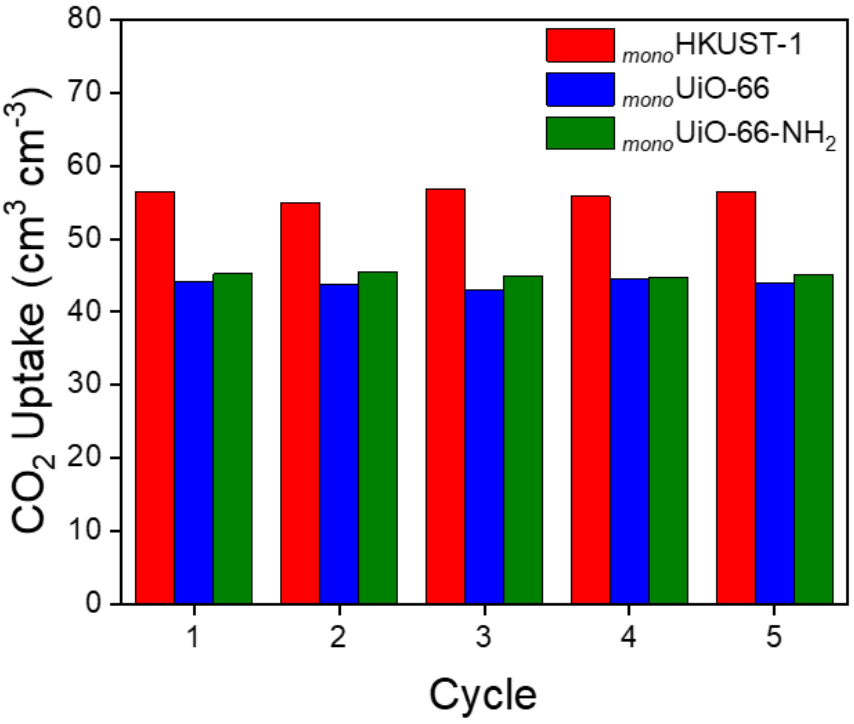

Figure S42: Cyclability of $_{mono}$MOFs in 50% CO_2/50% CH_4 *v/v* breakthrough studies, regeneration at 120 °C.

References

1. T. Tian, Z. Zeng, D. Vulpe, M. E. Casco, G. Divitini, P. A. Midgley, J. Silvestre-Albero, J. C. Tan, P. Z. Moghadam and D. Fairen-Jimenez, *Nat Mater*, 2018, **17**, 174-179.
2. B. M. Connolly, M. Aragones-Anglada, J. Gandara-Loe, N. A. Danaf, D. C. Lamb, J. P. Mehta, D. Vulpe, S. Wuttke, J. Silvestre-Albero, P. Z. Moghadam, A. E. H. Wheatley and D. Fairen-Jimenez, *Nat Commun*, 2019, **10**, 2345.
3. F. Raganati, V. Gargiulo, P. Ammendola, M. Alfe and R. Chirone, *Chem. Eng. J.*, 2014, **239**, 75-86.
4. J. H. Cavka, S. Jakobsen, U. Olsbye, N. Guillou, C. Lamberti, S. Bordiga and K. P. Lillerud, *Journal of the American Chemical Society*, 2008, **130**, 13850-13851.
5. M. Kandiah, M. H. Nilsen, S. Usseglio, S. Jakobsen, U. Olsbye, M. Tilset, C. Larabi, E. A. Quadrelli, F. Bonino and K. P. Lillerud, *Chemistry of Materials*, 2010, **22**, 6632-6640.
6. A. L. Myers and J. M. Prausnitz, *AIChE Journal*, 1965, **11**, 121-127.